Optical Properties of Lanthanide-doped $RbTiOAsO_4$ and Transition Metal-doped $KTiOPO_4$

Mark L. F. Phillips, Mark T. Anderson, and Michael B. Sinclair

Sandia National Laboratories, Albuquerque, NM 87185

Abstract:

We have synthesized derivatives of potassium titanyl phosphate (KTP) and rubidium titanyl arsenate (RTA) where Ti has been replaced by transition metal or lanthanide ions, and K, Ti, P or O has been replaced by aliovalent counterions. Up to 5 mol % lanthanide ion can be substituted onto the Ti sites in RTA, and 100 mol % substitution of other transition metals onto the Ti sites in KTP can be made. The visible spectra of these doped KTP phases are characteristic of the dopant ions, with sharp, narrow transitions resulting from lanthanide substitution and broader absorptions from transition-metal dopants. Powder second harmonic generation (SHG) intensities diminish with increased dopant concentration. Decreases in SHG intensities parallel those seen in previously studied systems. The choice of counterion substantially impacts some dopant solubilities, but generally affects SHG intensity and visible spectrum to a lesser degree. Single crystals doped with Er^{3+}, Fe^{3+} and Co^{2+} have linear absorption coefficients in the range of 1 to 5 cm^{-1}. Changes in noncritical phase matching wavelength due to anomalous dispersion are calculated to be less than 1 nm at the dopant levels tested.

This work was supported by the United States Department of Energy under Contract No. DE-AC04-94AL85000.

Introduction:

Potassium titanyl phosphate ($KTiOPO_4$, or KTP) is a nonlinear optical material renowned for efficiently frequency doubling near-IR laser sources such as 1.064 nm Nd:YAG.[1,2] This is due in part to KTP's large second order nonlinear optical coefficients and its capacity for angle-noncritical type II phase matching in the *x-y* plane between 990 and 1080 nm.[3] KTP is transparent from 4500 nm to 350 nm, so absorption will not interfere with second harmonic generation from pump wavelengths as short as 700 nm. However, efficient type II phase matching is not available in bulk KTP crystals at wavelengths shorter than 990 nm, and thus its utility as a doubler for shorter near-IR wavelengths (e.g., from Ti:sapphire and diode lasers) is limited.[4]

Loss of efficient phase matching in KTP at wavelengths shorter than 990 nm is caused by normal dispersion, which increases the refractive indices as an absorption band (e.g., a charge-transfer band, such as the one present below 350 nm in KTP) is approached from longer wavelengths. This in turn increases the amount of birefringence needed to phase match the fundamental (pump) and second harmonic (SH) wavelengths (Figure 1a).[5] We might overcome this effect by enhancing birefringence, or by altering the dispersion curve using anomalous dispersion. Anomalous dispersion refers to a decrease in refractive index with shorter wavelengths, and generally occurs in the presence of an absorption band. An absorption of sufficient oscillator strength can in principle alter the phase matching loci of a crystal, allowing noncritical phase matching (NCPM) at shorter wavelengths (Figure 1b). Anomalous dispersion phase matching (ADPM) has been demonstrated with solution phase organic dyes in electric field-induced second harmonic generation experiments.[6] If we are to use anomalous dispersion to shorten KTP's NCPM wavelength for type II phase matching, we need to introduce absorptions that are intense, but do not cause loss by overlapping onto the intended pump and second harmonic wavelengths. For diode laser or Ti:sapphire sources, pump wavelengths may range from 750 to 900 nm, and SH wavelengths from 375 to 450 nm.

We anticipate that doping metal ions with partially filled *d* or *f* orbitals into KTP or its isostructures will introduce absorptions into the visible spectrum of the host phase. It has been shown that small quantities of Fe dopant (<1 wt %) in $KTiOAsO_4$ can substantially blue-shift the NCPM wavelength of this material by enhancing its birefringence.[7] This project will determine the effects of lanthanide and transition metal dopants on phase matching loci of KTP and its isostructures. We report here the results from our tests of the feasibility of using ADPM to alter NCPM wavelengths in the $KTiOPO_4$ structure type.

The presence of three different cationic positions (K, Ti, and P) in the KTP structure potentially offers three different sites onto which lanthanide or transition metal ions may be doped. Previous results

have shown that other transition metals such as Fe[8] and V,[9] and main group metals such as Ga[10] and Sn[11,12] can partially or completely replace Ti in KTP. Complete substitution for Ti is accompanied by a nearly total loss of SHG intensity. In the case of Fe, Ga, and Sn this is attributed to loss of the distortion of the MO_6 groups that is essential to optical nonlinearity in KTP and its isostructures. However, the VO_6 groups in $KVOPO_4$ retain the distortion that is characteristic of the TiO_6 groups in KTP, and the low SHG intensity of $KVOPO_4$ when tested with 1.064 μm pump radiation may be caused instead by optical absorption at both the fundamental and second harmonic wavelengths. Partial replacement of Ti can leave the resulting phase with considerable SHG intensity; for example, 30 mol % substitution of Ga in KTP reduces SHG intensity by only a factor of two. In contrast, complete Ga substitution reduces SHG intensity by a factor of one thousand.[10]

As dopants, lanthanides have the advantage of narrow absorption bands in the visible, reducing the possibility of overlap with the desired pump and output beams. While transition metals generally have broader absorptions in the visible spectrum, their ionic radii are similar to that of Ti and should thus be more soluble in KTP than lanthanides. It has already been observed that Ln^{3+} ions are poorly soluble in $KTiOPO_4$ and that $RbTiOAsO_4$ is the preferred host for these dopants.[13] Transition metals can in principle also be substituted into the tetrahedral sites normally occupied by phosphorus, if the dopant ions are sufficiently small and high-valent. It is possible that if the dopant replaces P rather than Ti, SHG intensity will be affected to a lesser degree. It is unlikely that the potassium sites in KTP will be suitable for dopant siting, since solubilities of divalent and trivalent ions on the K sites in excess of 1% have not been reported.[14]

Aliovalent substitutions, such as replacing Ti^{4+} with Ln^{3+}, must be compensated by either creating vacancies elsewhere in the structure (e.g., on either the potassium or oxygen sublattices), or by simultaneously substituting a counterion elsewhere in the structure to balance charge. Counterions can, in principle, be substituted onto the K, Ti, P, and oxygen sites that link the TiO_6 groups. As with the dopant ions, it appears reasonable that substituting counterions into sites outside of the TiO_6 groups should reduce their impact on SHG intensity. Suitable counterions for divalent and trivalent dopants may include Sr^{2+} and Ba^{2+} (on the K sites), Nb(V) (on the Ti sites), F^- (on the linking oxygen sites), and S(VI), Se(VI), Mo(VI), W(VI), and Re(VII) (on the P sites).

We have surveyed the optical properties of doped KTP and RTA by synthesizing these new phases as powders, both from solid state and solution precursors, and collecting UV-visible spectra and powder SHG intensities. We then used these data to target optimum phases for ADPM study; these phases were then grown as single crystals and used for measuring absorption coefficients. We report here the effects of identity and concentration of dopant and counterion on dopant solubilities, UV-visible

spectra, and SHG intensities of lanthanide- and transition metal-doped KTP and RTA. Using absorption data from doped KTP and RTA single crystals, we can predict the effect of anomalous dispersion on NCPM wavelength.

Experimental:

Synthesis:

Both lanthanide-doped RTA and transition metal-doped KTP powders were prepared via either solid state or hydrothermal routes. Solid state preparations were made by sintering oxides or oxide precursors of Ti and the dopant metal with RbH_2AsO_4 overnight at 600°C, then grinding and reheating at 800-950 °C. Samples were reground and reheated as necessary until reactions were complete. Hydrothermally prepared samples were synthesized by mixing soluble sources of Ti, dopant, and counterion with aqueous potassium phosphate or rubidium arsenate. These were then autoclaved in water at 200 °C at autogenous pressure for several days, then recovered by filtration.

Single crystals of doped KTP and RTA phases were prepared by dissolving TiO_2, dopant metal oxide or oxide precursor, and counterion in a rubidium arsenate or potassium phosphate flux. Crystals precipitated via spontaneous nucleation when a saturated flux was cooled. Typical saturation temperatures were 900-950 °C. Excess flux was removed with hot water, and the crystals were recovered by filtration. Crystals containing volatile cations (such as sulfate) were synthesized hydrothermally by dissolving TiO_2, dopant metal nitrate, and counterion in an aqueous rubidium arsenate or potassium phosphate flux at 650 °C and 3000 bar. Again, crystals of the doped phase spontaneously nucleated and precipitated as the reaction mixture was cooled.

Characterization:

Purity of the product phases was determined by X-ray powder diffraction, using a Scintag automated diffractometer with a Cu Kα (λ = 1.5406 Å) X-ray source. Particle size distributions were measured using a Horiba Model CAPA-700 particle size analyzer. Spectral data were collected from lanthanide-doped RTA powder samples in diffuse reflectance using a Cary 14 UV-visible-IR spectrophotometer. A Cary 5E UV-visible-IR spectrophotometer with an integrating sphere accessory was used to collect hemisperical reflectance data from transition metal-doped KTP samples.

Spectral data from single crystals were collected in transmission. Light from a tungsten-halogen lamp was passed through a chopper, then an aperture of smaller diameter than the face of the crystal. The light was focused onto the crystal, recollimated, and introduced into a scanning monochromator. The signal was detected with a photomultiplier tube and analyzed using a lock-in amplifier.

Powder SHG intensity data were obtained at 1064 nm using a system similar to that described by Dougherty and Kurtz.[15] A Spectra-Physics DCR11-3D Nd:YAG laser was the source of 1.064 μm light, producing 300 mJ, 8 ns pulses at a repetition rate of 2 Hz. SH light from the samples was collected with an elliptical reflector, separated from the fundamental by a dichroic mirror, and introduced into a grating monochromator. The SH light was detected with a Hamamatsu 1P28A photomultiplier tube. Signals from each sample were measured and averaged over 20 shots using a Tektronix 2467B 400 MHz oscilloscope with a DCS01 digitizing camera system.

Results:

Powder studies:

The solubilities of the dopants in KTP and RTA were estimated from the powder X-ray diffraction results. Regardless of the counterion used, solubilities of lanthanide (III) ions in KTP were no greater than 0.5 mol %, and may be less. Approximately 5 mol % of the later lanthanides (Er-Lu) could be substituted onto the Ti sites in RTA. In general, lanthanide solubilities decreased with increasing ionic radius or decreasing atomic number. It is noteworthy that the highest solubilities were obtained with samples prepared via solid state, rather than hydrothermally (Figure 2). This may be due to higher defect concentrations in the samples prepared at high temperatures.[13] The choice of counterion has a secondary effect on lanthanide solubility.

Solubilities of transition metals in KTP are also controlled by selection of dopant and counterion, though in general, they are much more soluble than the lanthanides (Figure 3). This is not too surprising in light of the previously mentioned 100 mol % solubility of Fe(III), V(IV), and Ga(III). Again, the solubility limit is governed by both the dopant and counterion. Data reported in Figure 3 should be regarded as minimum solubilities, since it may be possible to increase dopant concentrations by changing hydrothermal processing parameters. Not shown are solubility data for Ni(II) and Cu(II) on the Ti sites or for V(V) and Cr(VI) on the P sites. Hydrothermal solubility limits for Ni and Cu are estimated to lie between 10-20 mol % and 5-10 mol %, respectively, with F^-, S(VI) and Re(VII) counterions. Compositions containing 15 mol % Cr(VI) and 40 mol % V(V) could be made as pure phases via the solid state.

The UV-visible spectra were generally characteristic of the dopant ions (Figures 4, 5). In both the lanthanide-doped RTA and transition metal-doped KTP phases the counterion can shift the midpoint of the charge-transfer band, but does not influence the visible spectrum. From these data we note that suitable dopants for crystals intended for frequency doubling to wavelengths shorter than 450 nm include Er, Co, and possibly Fe.

SHG intensities decreased exponentially with dopant concentration in RTA:Ln,Nb phases prepared via solid state routes (Figure 6). The doped KTP and RTA samples prepared hydrothermally showed more complicated behavior, with some counterions causing an increase in SHG intensity at low dopant concentrations, then reducing it at increased dopant levels (Figure 7). The reduction of SHG intensity with substitution of other metals for Ti agrees with theory.[9,10] The increased SHG intensities at low dopant concentrations are attributable to changes in particle size distribution.[15] The distribution of particle sizes in some of the lightly doped phases includes a higher concentration of larger particles, (Figure 8) which contribute disproportionately to the bulk SHG signal. At higher dopant concentrations SHG intensity falls off more dramatically when Nb is used as a counterion. We note that Nb also replaces Ti, and in order to dope in x mole percent Ln(III), $2x$ Ti must be removed. We conclude that Nb does not contribute to second order nonlinearity in the RTA structure.

Among the transition metal-doped KTP samples, it appears that Co substitution is more deleterious to SHG intensity than Fe or Cr substitution. While it is conceivable that a given concentration of a divalent ion in KTP may have a larger impact on SHG intensity than the equivalent concentration of trivalent ions, it is more likely that the relative loss of SHG intensity is due to absorption at 532 nm by the Co^{2+} ions (Figure 5). Similarly, absorption may be responsible for the low SHG intensities of KTP doped with V(V) and Cr(VI); the SHG intensities of $KTiOP_{0.8}V_{0.2}O_4$ and $KTiOP_{0.8}Cr_{0.15}Zn_{0.05}O_4$ are 0.06 and 0.01 times that of undoped KTP, respectively.

From the dopant solubility, spectral, and SHG intensity data, we conclude that:
a.) the choice of dopant ion determines solubility and absorption spectrum,
b.) except where the dopant absorbs SH light, SHG intensity depends primarily on the amount of Ti remaining in the host, and not on the dopant chosen, and
c.) the counterion affects dopant solubility, charge-transfer band position, and in hydrothermally synthesized powders, the particle size distribution.

Based on these data, the most promising lanthanide dopant is Er, principally due to its high solubility in RTA (compared with Pr or Nd). The most promising transition metal dopants are Fe and Co. Acceptable counterions for each of these dopants include F^-, S(VI), Se(VI), Mo(VI), W(VI), and Re(VII).

Single crystal studies:

Single crystals of doped KTP and RTA phases possessed the typical prismatic KTP habit, and were up to 2 mm long and 0.8 mm thick. Many crystals had flat faces with at least 1 mm^2 aperture; these were deemed suitable for use in collecting transmission spectra. All crystals were colored, some intensely so.

Er-doped RTA crystals were grown using Nb(V), F^-, Mo(VI), and W(VI) as counterions, while Fe and Co-doped KTP crystals were grown using F^-, S(VI), and Re(VII) as counterions.

Transmission spectra obtained from these crystals (Figure 9) reveal narrower transitions than those seen in diffuse or hemispherical reflectance spectra. In the cases of the Fe and Co-doped KTP crystals the *d-d* and charge-transfer transitions are shifted closer together. From the transmittance data and the crystal thicknesses we calculated linear absorption coefficients, which for transitions between 400 and 900 nm were all between 1 and 5 cm^{-1}.

Using a calculated relationship between NCPM wavelength shift and absorption coefficient (Figure 10), we estimate that the blue-shift in NCPM wavelength caused by anomalous dispersion in the doped crystals synthesized thus far will be less than 1 nm. However, the effects of the dopants on birefringence in KTP and RTA (other than those due to anomalous dispersion) are not known at this time, and increased birefringence may favorably alter NCPM wavelengths. Refractive indices and phase matching loci of our doped KTP and RTA crystals will be reported shortly.

Acknowledgments:

This work was supported by the United States Department of Energy under Contract No. DE-AC04-94AL85000. We thank Diana Lamppa (SNL) for her assistance in collecting the particle size data, and Rod Mahoney and Herb Tardy (SNL) for collecting the hemispherical reflectance UV-visible data.

References:

1. R. F. Belt, G. Gashurov, Y. S. Liu, "KTP as a Harmonic Generator for Nd:YAG Lasers", *Laser Focus/Electro-Optics* 21(10), pp. 110-124, 1985.

2. J. C. Jacco, "$KTiOPO_4$ (KTP): Past, Present and Future", *Proc. SPIE* 968, pp. 93-99, 1988.

3. F. C. Zumsteg, J. D. Bierlein, and T. E. Gier, "$K_xRb_{1-x}TiOPO_4$: A New Nonlinear Optical Material", *J. Appl. Phys.* 47, pp. 4980-4985, 1976.

4. Type I phase-matched SHG in segmented KTP waveguides has yielded output wavelengths as short as 0.38 nm. See C. J. van der Poel, J. D. Bierlein, J. B. Brown, and S. Colak, "Efficient Type I Blue Second-harmonic Generation in Periodically Segmented $KTiOPO_4$ Waveguides", *Appl. Phys. Lett.* 57, pp. 2074-2076, 1990.

5. Dispersion curves in Figure 1 were calculated using Sellmeier coefficients reported in H. Vanherzeele, J. D. Bierlein, and F. C. Zumsteg, *Appl. Opt.* 27, pp. 3314-3316, 1988.

6. P. A. Cahill, K. D. Singer, and L. A. King, "Anomalous-dispersion Phase-matched Second Harmonic Generation", *Opt. Lett.* 14, pp. 1137-1139, 1989.

7. L. K. Cheng, L.-T. Cheng, J. D. Bierlein, F. C. Zumsteg, and A. A. Ballman, "Properties of Doped and Undoped Crystals of Single Domain $KTiOAsO_4$", *Appl. Phys. Lett.* 62, pp. 346-348, 1993.

8. E. N. Matvienko, O. V. Yakubovich, M. A. Simonov, and M. A. Belov, "Crystal Structure of Potassium Iron (3+) Orthophosphate ($KFePO_4F$)", *Dokl. Akad. Nauk SSSR* 246, pp. 875-878, 1979.

9. M. L. F. Phillips, W. T. A. Harrison, T. E. Gier, G. D. Stucky, G. V. Kulkarni, and J. K. Burdett, "Electronic Effects of Substitution Chemistry in the $KTiOPO_4$ Structure Field: Structure and Optical Properties of Potassium Vanadyl Phosphate", *Inorg. Chem.* 29, pp. 2158-2163, 1990.

10. G. D. Stucky, M. L. F. Phillips, and T. E. Gier, "The Potassium Titanyl Phosphate Structure Field: A Model for New Nonlinear Optical Materials", *Chem. Mater.* 1, pp. 492-509, 1989.

11. R. H. Jarman and S. G. Grubb, "Isomorphous Substitution in Potassium Titanyl Phosphate", *Proc. SPIE* 968, pp. 108-111, 1988.

12. M. L. F. Phillips, W. T. A. Harrison, and G. D. Stucky, "Influence of Electronic Configuration on the Structure and Optical Properties of $KSnOPO_4$", *Inorg. Chem.* 29, pp. 3245-3247, 1990. 13. M. T. Anderson, M. L. F. Phillips, and G. D. Stucky, "Inorganic Materials for Anomalous-Dispersion Phase-Matched Second Harmonic Generation: Rubidium Titanyl Arsenate Isomorphs, $Rb[Ti_{1-2x}Ln_xNb_x]OAsO_4$", *J. Non-Cryst. Sol.* 1994, in press.

14. M. G. Roelofs, P. A. Morris, and J. D. Bierlein, "Ion Exchange of Rb, Ba, and Sr in $KTiOPO_4$", *Appl. Phys. Lett.* 70, pp. 720-728, 1991.

15. J. P. Dougherty and S. K. Kurtz, "A Second Harmonic Analyzer for the Detection of Non-Centrosymmetry", *J. Appl. Cryst.* 9, pp. 145-157, 1976.

Figure captions:

Figure 1: a. Normal dispersion curves for KTP, showing type II phase matching in the x-y plane.
b. Hypothetical type II phase matching after introducing a Lorentzian absorption centered at 625 nm with a linear absorption coefficient of 2.00×10^4 cm^{-1} and a line width of 10 nm (FWHM).

Figure 2: Variation of of Er^{3+} solubility in RTA with counterion, synthetic method.

Figure 3. Solubilities of transition metal dopants in KTP with various counterions. All phases were prepared hydrothermally at 200 °C.

Figure 4: Diffuse-reflectance spectra of solid state-synthesized RTA:Er,Nb samples at several dopant concentrations.

Figure 5: Hemispherical-reflectance spectra of transition metal-doped KTP.

Figure 6: Effect of Ln^{3+} doping on SHG intensity in solid state-synthesized RTA:Ln,Nb.

Figure 7: a. SHG intensity vs. Er^{3+} concentration in hydrothermally prepared RTA.
b. SHG intensity vs. Cr^{3+}, Co^{2+} concentration in hydrothermally prepared KTP. Several different counterions were used in both the KTP and RTA samples. The uncertainty in SHG intensity values is estimated to be 10%.

Figure 8: a. Particle size distribution in hydrothermal RTA:Er,S as function of dopant concentration.
b. Particle size distributions of hydrothermal KTP, KTP:Cr,S (2 mol %), KTP:Co,S (2 mol %).

Figure 9: Transmission spectra of a.) RTA:Er,W; b.) KTP:Fe,F; c.)KTP:Co,Re.

Figure 10: Noncritical phase matching wavelength in KTP vs. linear absorption coefficient (α) caused by transitions centered at 510, 640 and 790 nm, with intensity ratios of 1, 0.5, and 0.33, respectively, and line widths of 10 nm (FWHM). α refers to the linear absorption coefficient of the most intense peak (510 nm).

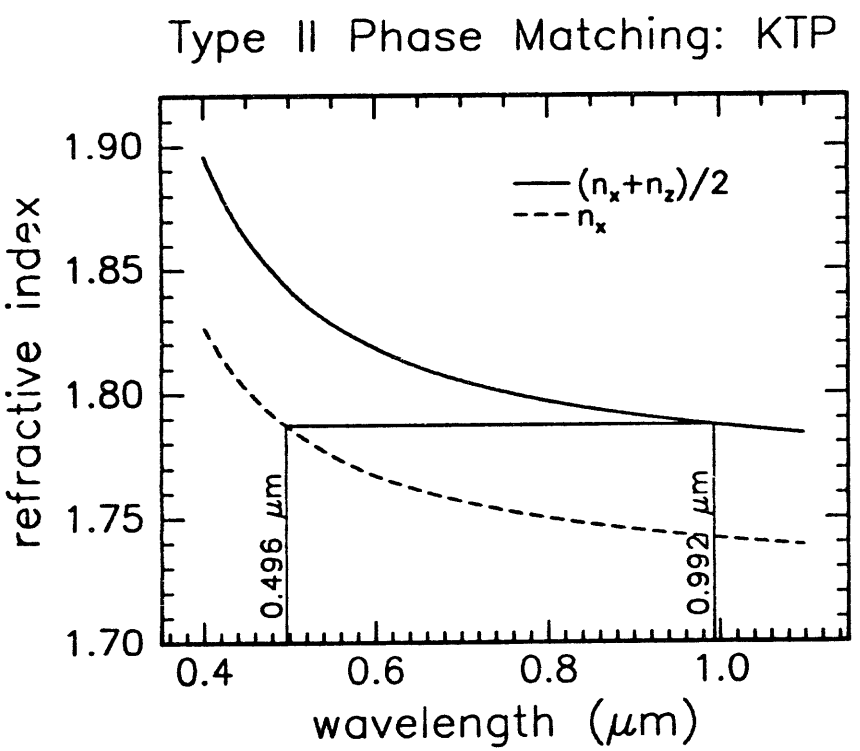
Type II Phase Matching: KTP
refractive index
1.90
1.85
1.80
1.75
1.70
0.4
0.6
0.8
1.0
wavelength (μm)
(nx+nz)/2
nx
0.496 μm
0.992 μm

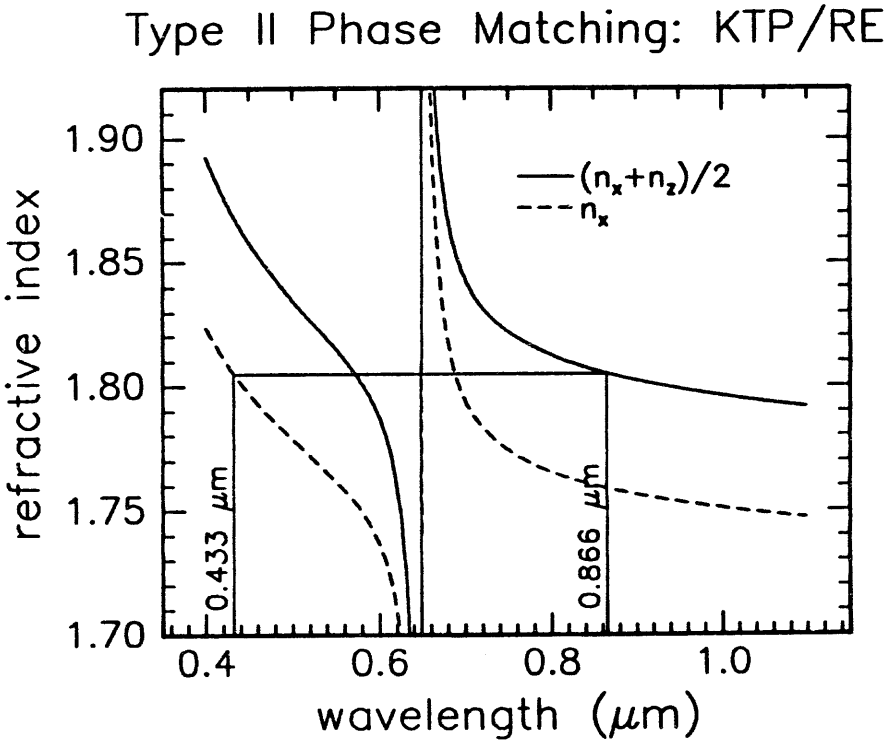
Type II Phase Matching: KTP/RE
refractive index
1.90
1.85
1.80
1.75
1.70
0.4
0.6
0.8
1.0
wavelength (μm)
(nx+nz)/2
nx
0.433 μm
0.866 μm

Figure 1

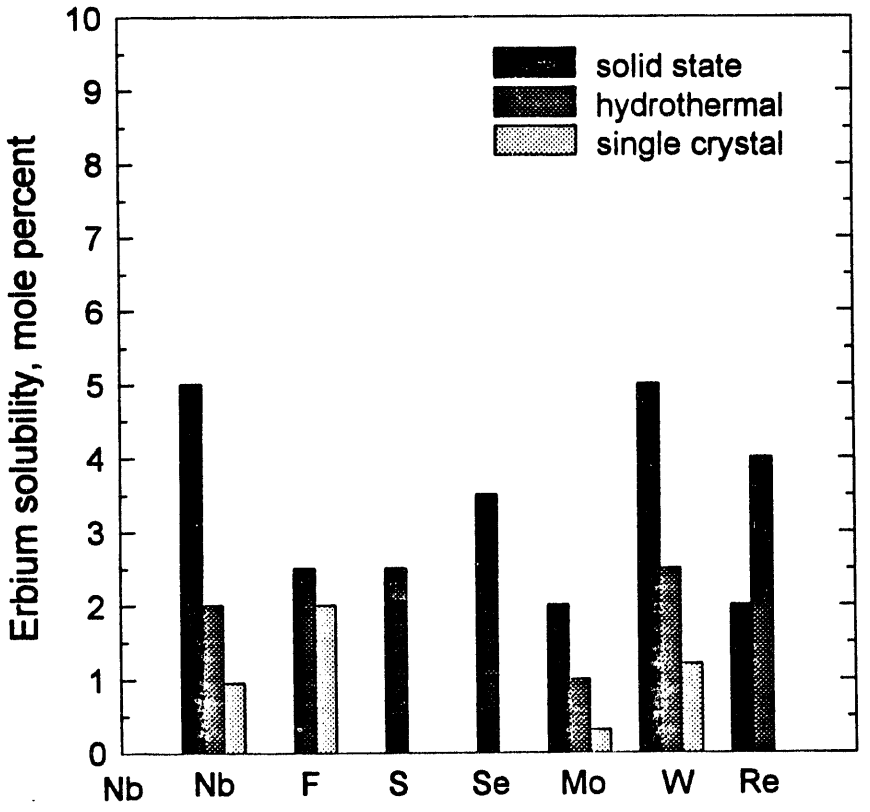
Erbium solubility, mole percent
10
9
8
7
6
5
4
3
2
1
0
solid state
hydrothermal
single crystal
Nb
Nb
F
S
Se
Mo
W
Re

Figure 2

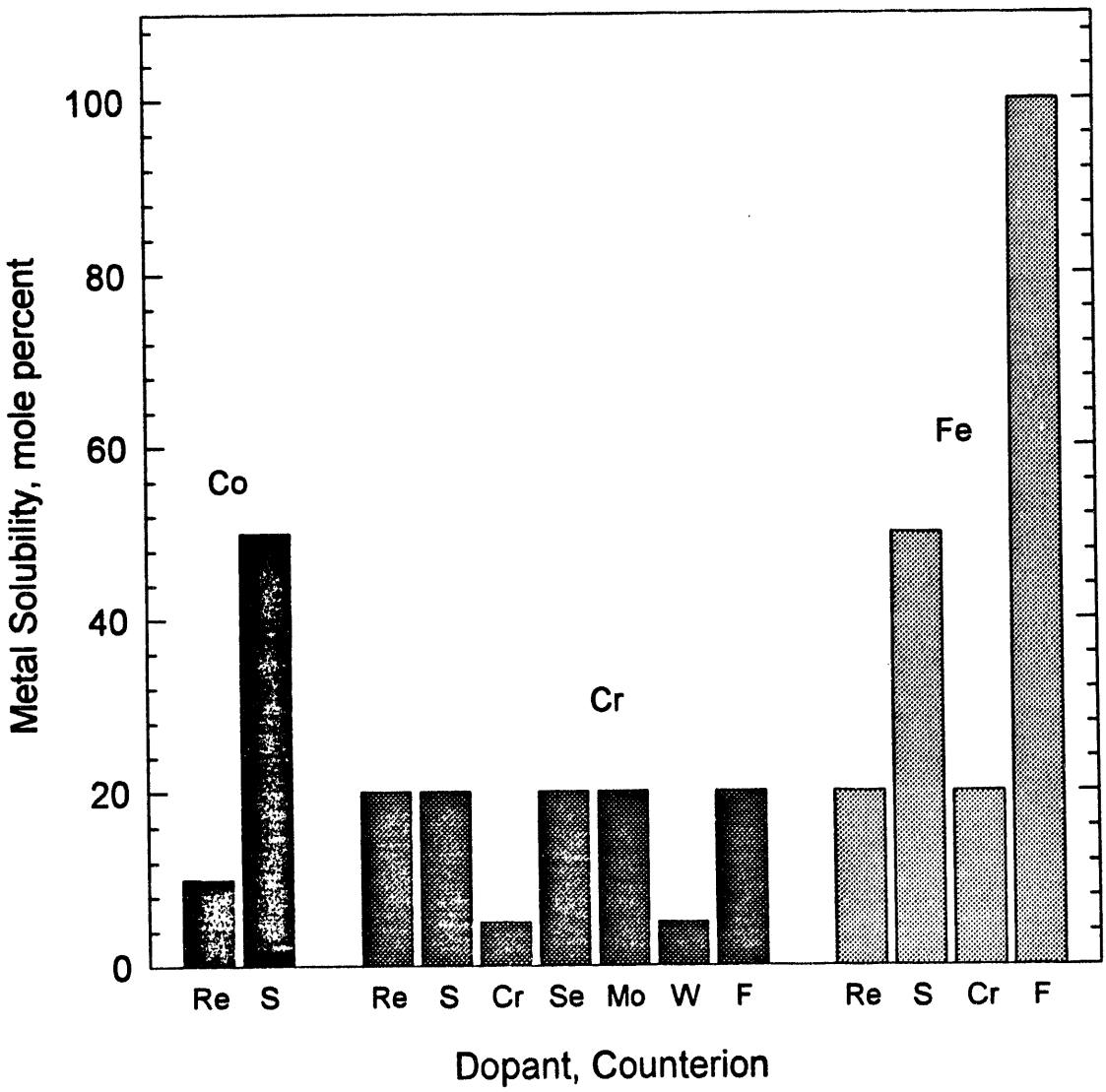
Metal Solubility, mole percent
100
80
60
40
20
0
Co
Cr
Fe
Re S
Re S Cr Se Mo W F
Re S Cr F
Dopant, Counterion

Figure 3

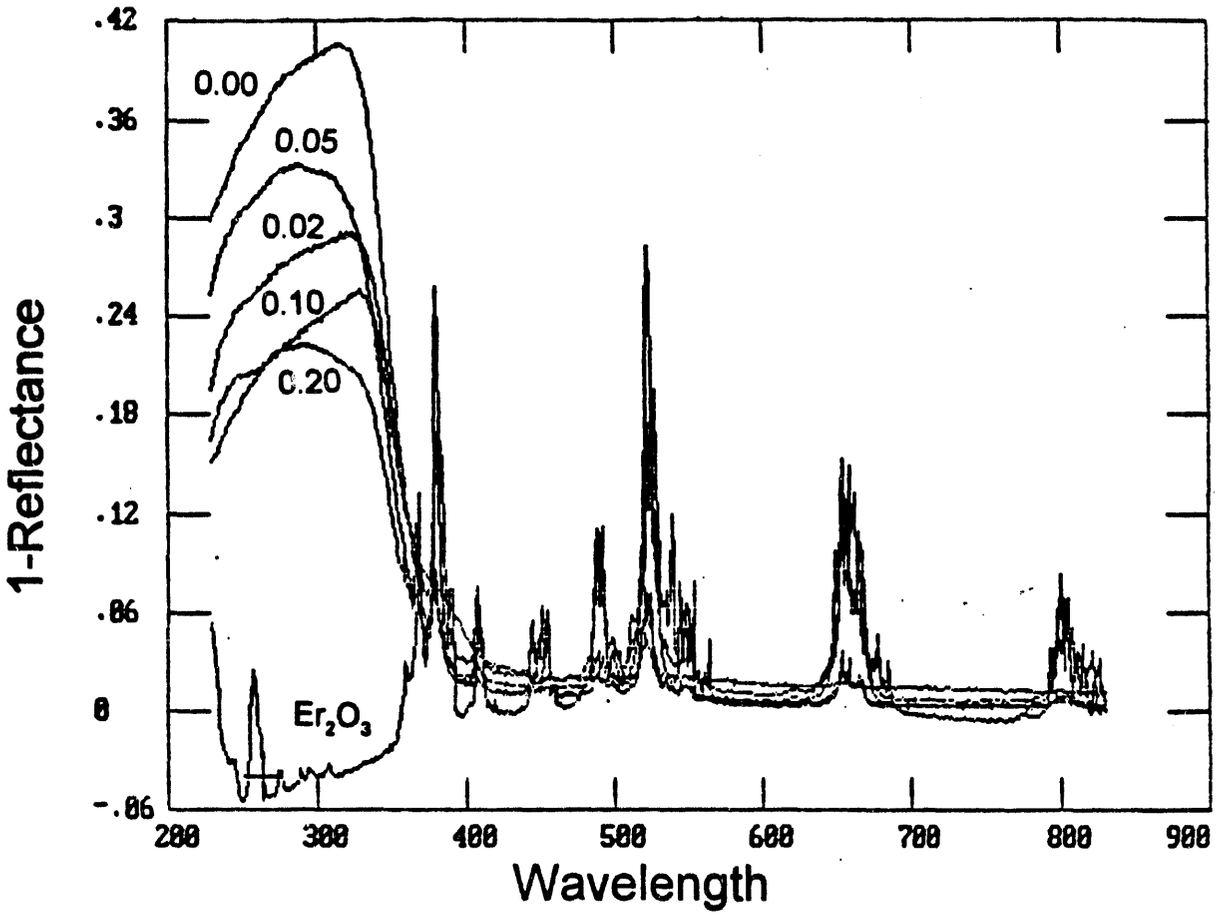
.42
.36
.3
.24
.18
.12
.06
0
-.06
0.00
0.05
0.02
0.10
0.20
Er_2O_3
200
300
400
500
600
700
800
900
1-Reflectance
Wavelength

Figure 4

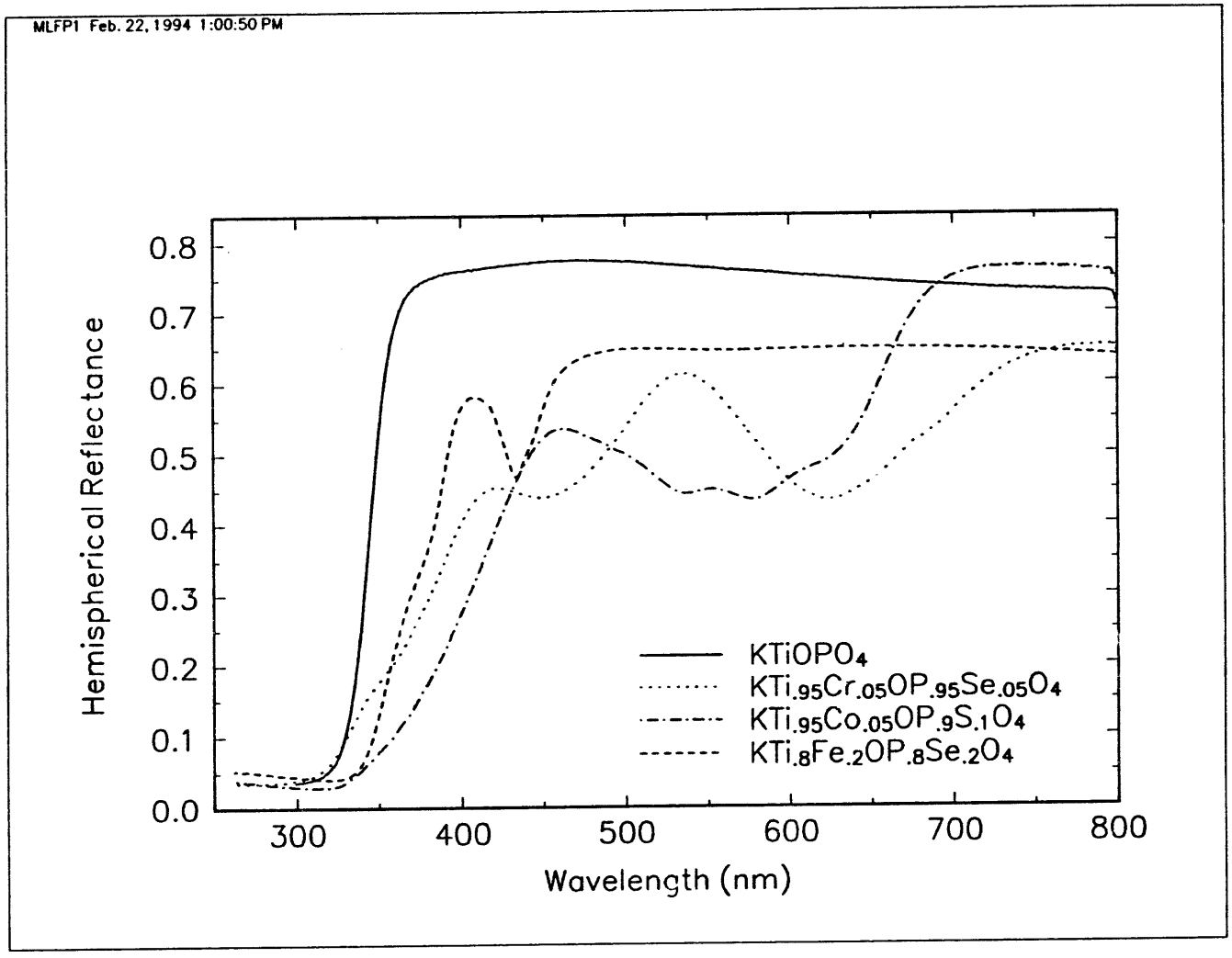
MLFP1 Feb. 22, 1994 1:00:50 PM
Hemispherical Reflectance
0.0
0.1
0.2
0.3
0.4
0.5
0.6
0.7
0.8
300
400
500
600
700
800
Wavelength (nm)
KTiOPO4
KTi.95Cr.05OP.95Se.05O4
KTi.95Co.05OP.9S.1O4
KTi.8Fe.2OP.8Se.2O4

Figure 5

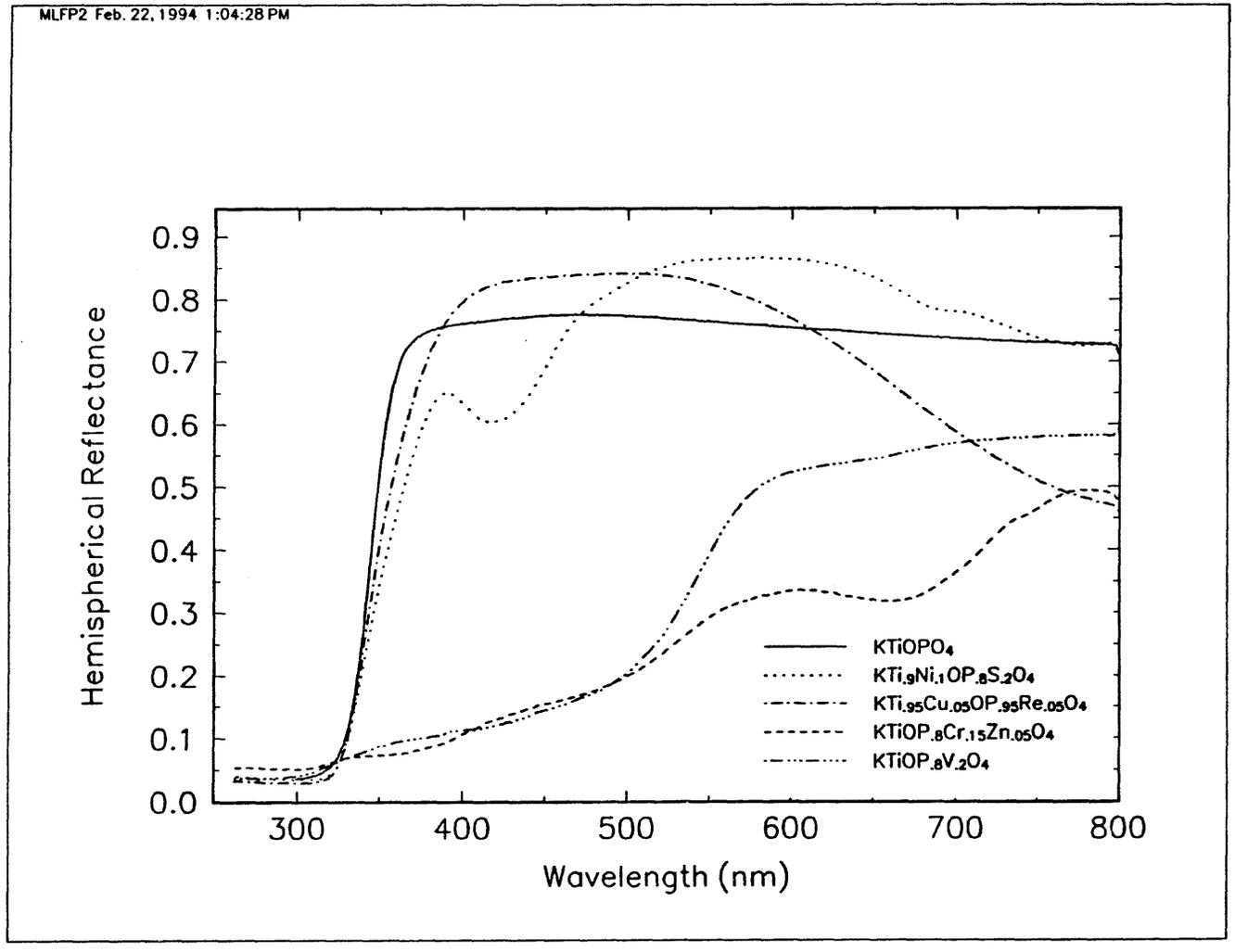
MLFP2 Feb. 22, 1994 1:04:28 PM
Hemispherical Reflectance
0.0
0.1
0.2
0.3
0.4
0.5
0.6
0.7
0.8
0.9
300
400
500
600
700
800
Wavelength (nm)
KTiOPO4
KTi.9Ni.1OP.8S.2O4
KTi.95Cu.05OP.95Re.05O4
KTiOP.8Cr.15Zn.05O4
KTiOP.8V.2O4

Figure 5

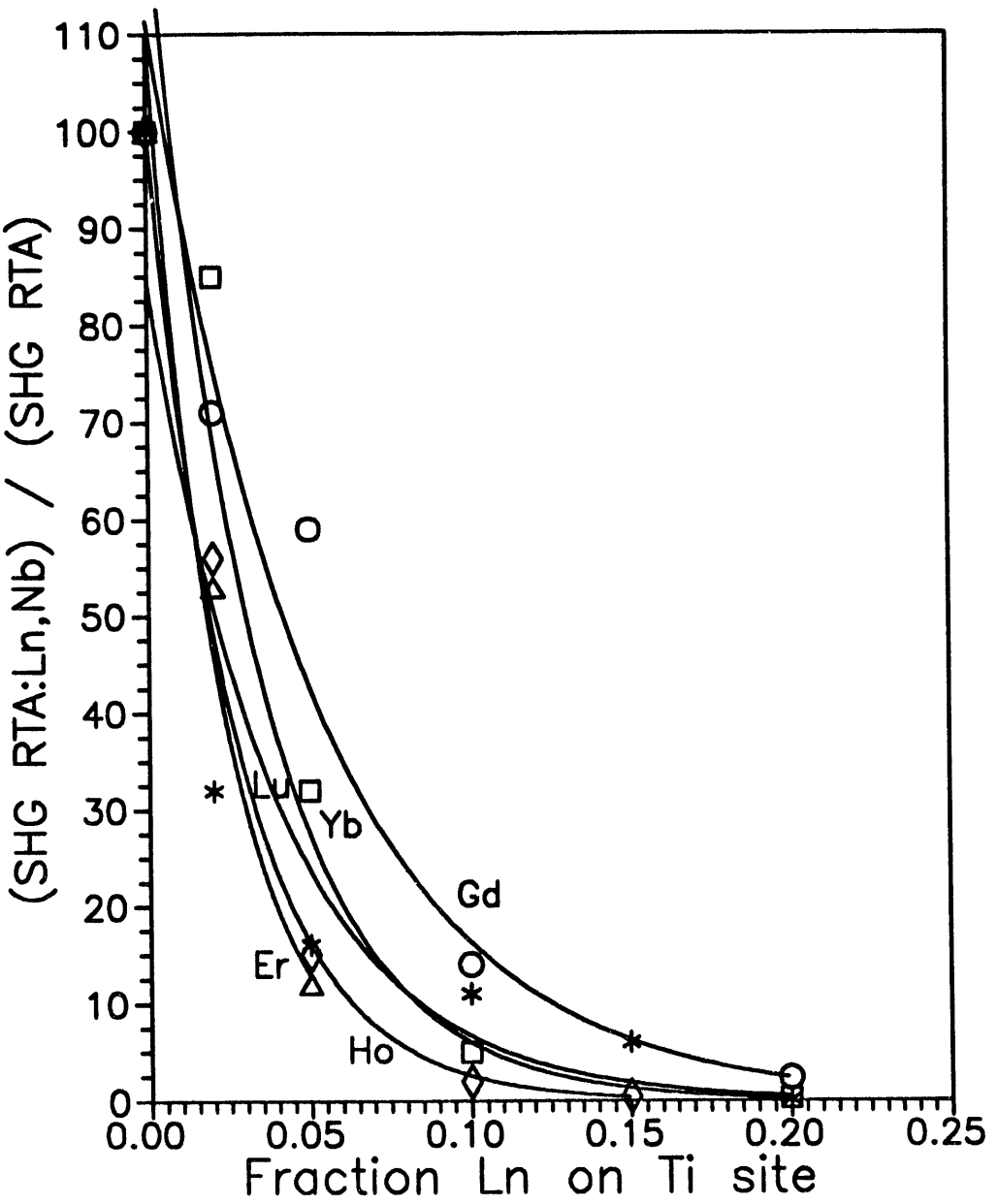
(SHG RTA:Ln,Nb) / (SHG RTA)
Fraction Ln on Ti site
110
100
90
80
70
60
50
40
30
20
10
0
0.00
0.05
0.10
0.15
0.20
0.25
Lu
Yb
Gd
Er
Ho

Figure 6

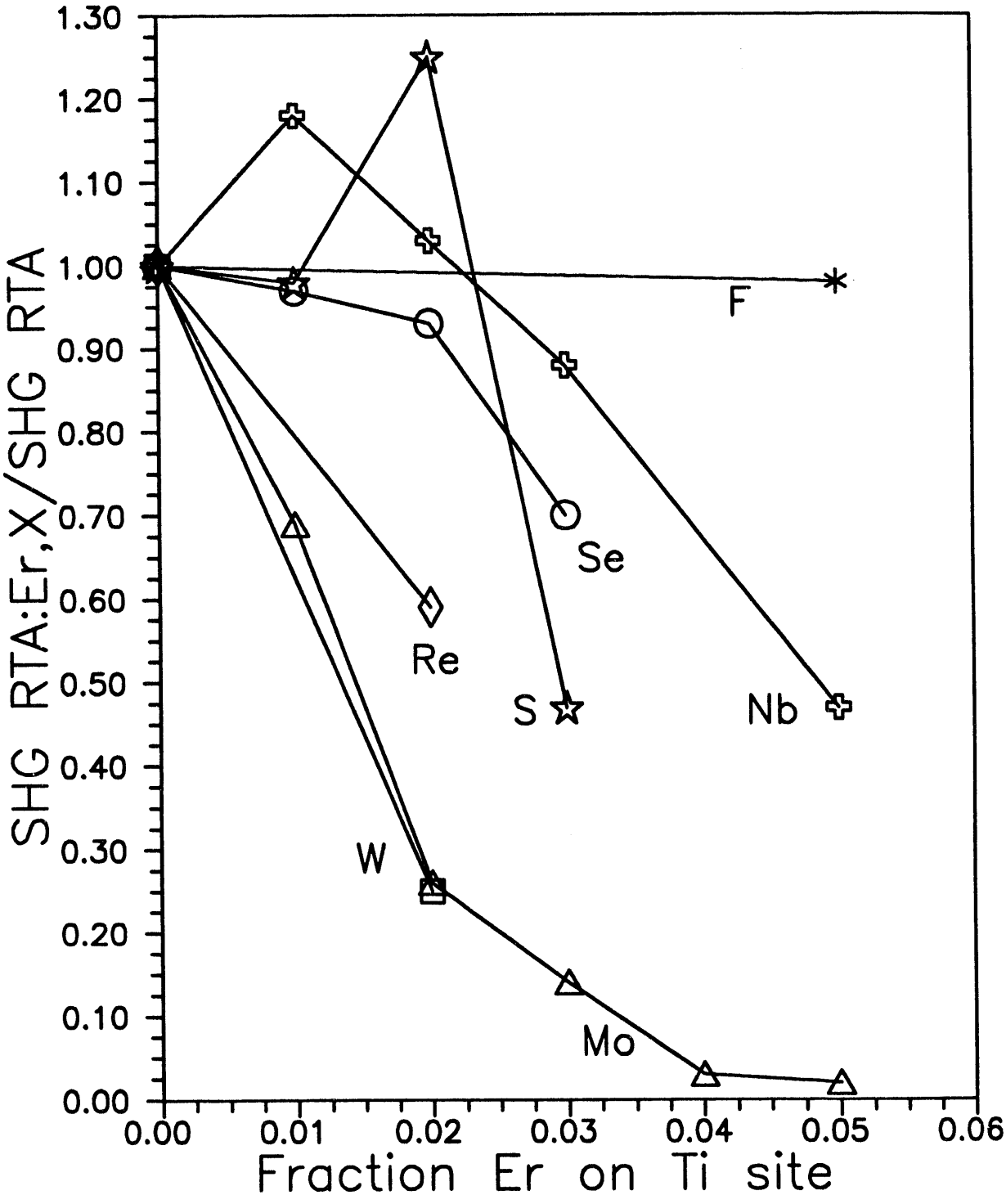
SHG RTA:Er,X/SHG RTA
1.30
1.20
1.10
1.00
0.90
0.80
0.70
0.60
0.50
0.40
0.30
0.20
0.10
0.00
0.00
0.01
0.02
0.03
0.04
0.05
0.06
Fraction Er on Ti site
F
Se
Re
S
Nb
W
Mo

Figure 7a

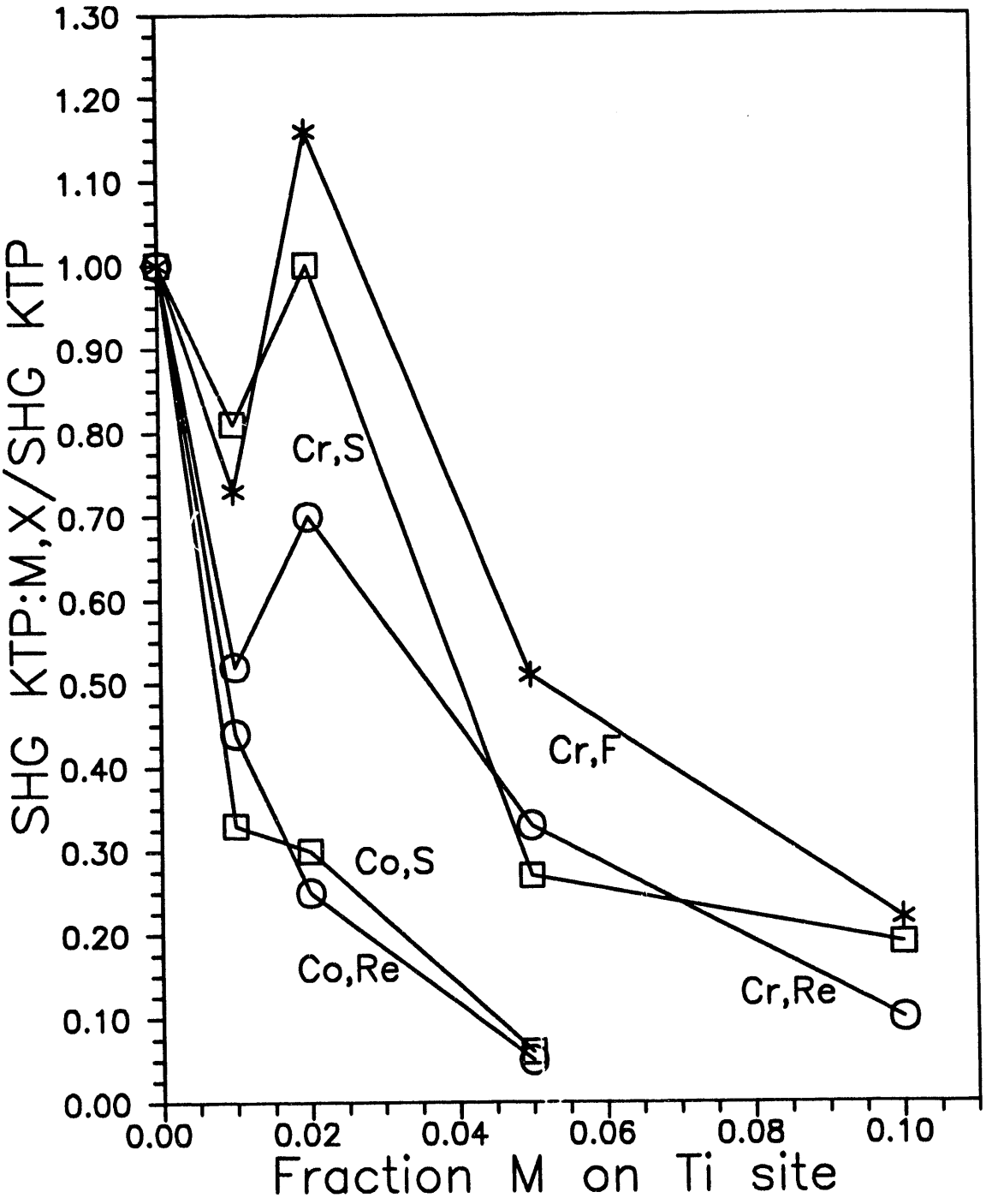
SHG KTP:M,X/SHG KTP
1.30
1.20
1.10
1.00
0.90
0.80
0.70
0.60
0.50
0.40
0.30
0.20
0.10
0.00
0.00
0.02
0.04
0.06
0.08
0.10
Fraction M on Ti site
Cr,S
Cr,F
Co,S
Co,Re
Cr,Re

Figure 7b

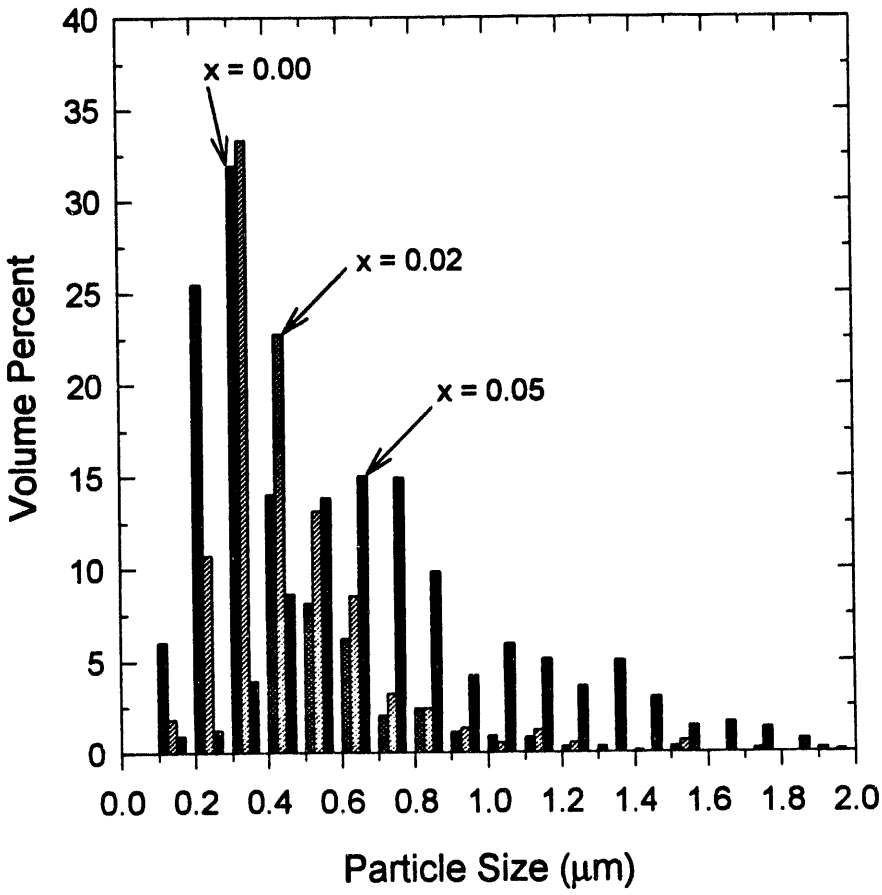
40
35
30
25
20
15
10
5
0
Volume Percent
x = 0.00
x = 0.02
x = 0.05
0.0
0.2
0.4
0.6
0.8
1.0
1.2
1.4
1.6
1.8
2.0
Particle Size (μm)

Figure 8a

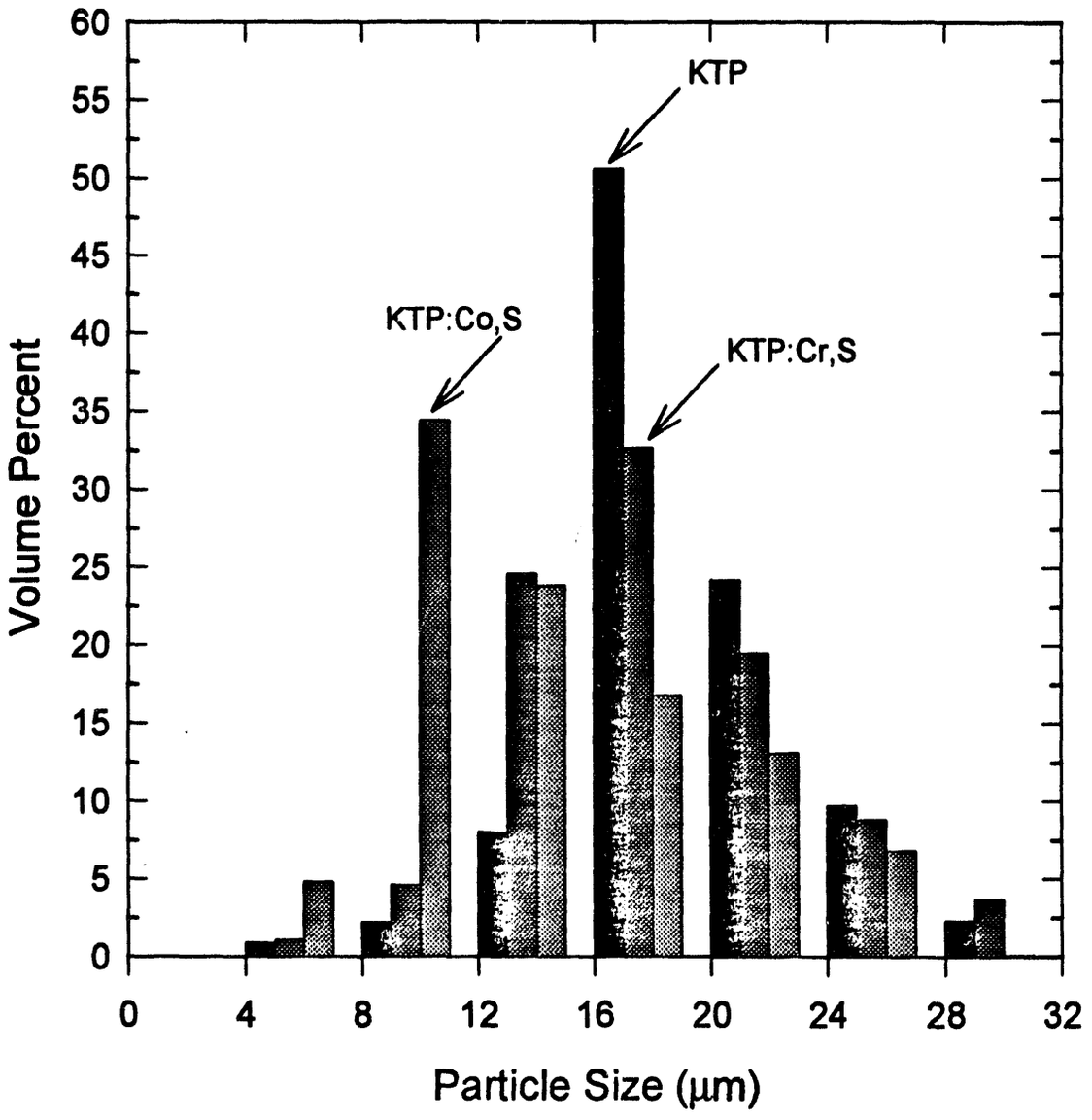
60
55
50
45
40
35
30
25
20
15
10
5
0
Volume Percent
KTP
KTP:Co,S
KTP:Cr,S
0
4
8
12
16
20
24
28
32
Particle Size (μm)

Figure 8b

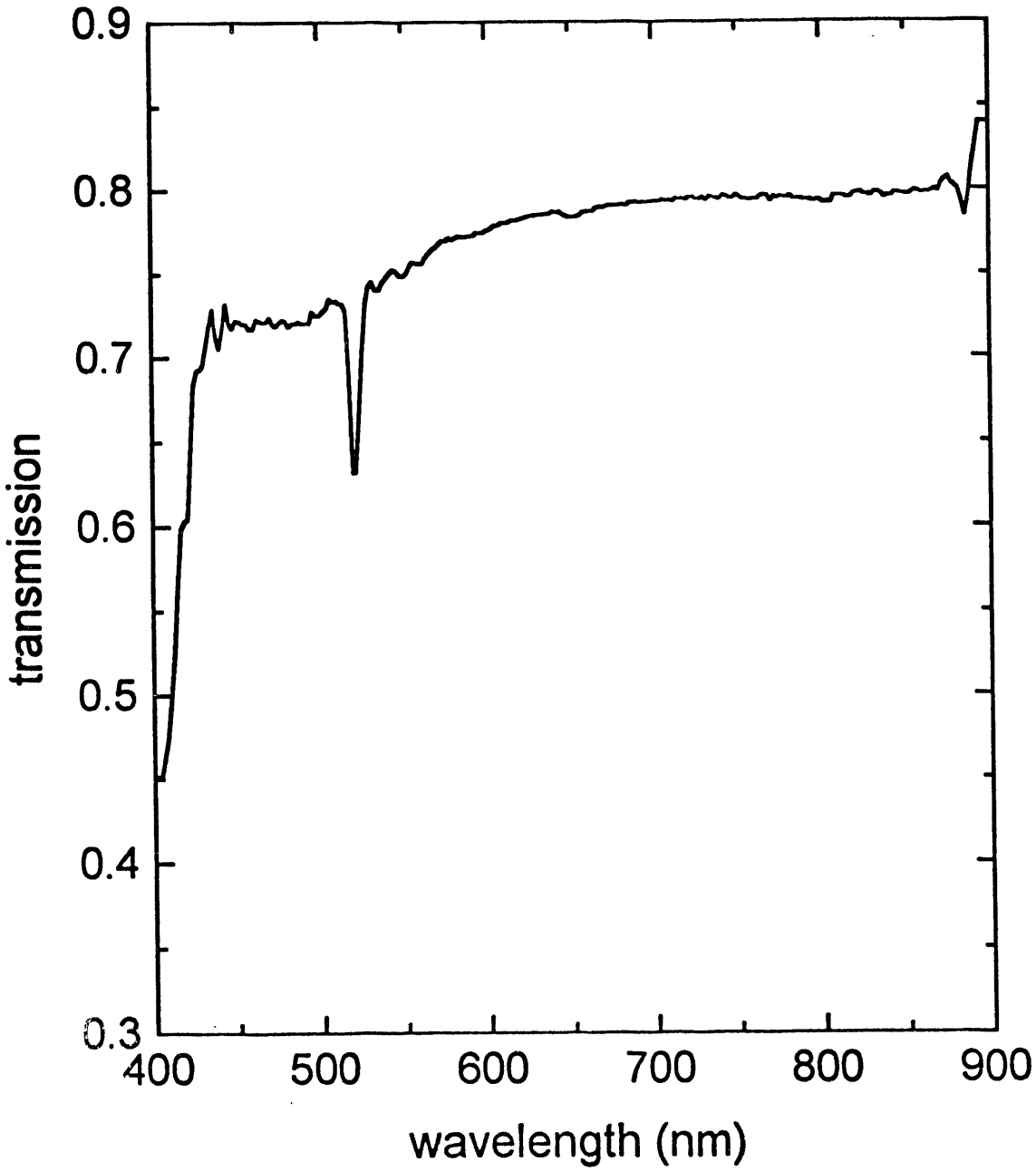
0.9
0.8
0.7
0.6
0.5
0.4
0.3
transmission
400
500
600
700
800
900
wavelength (nm)

Figure 9a

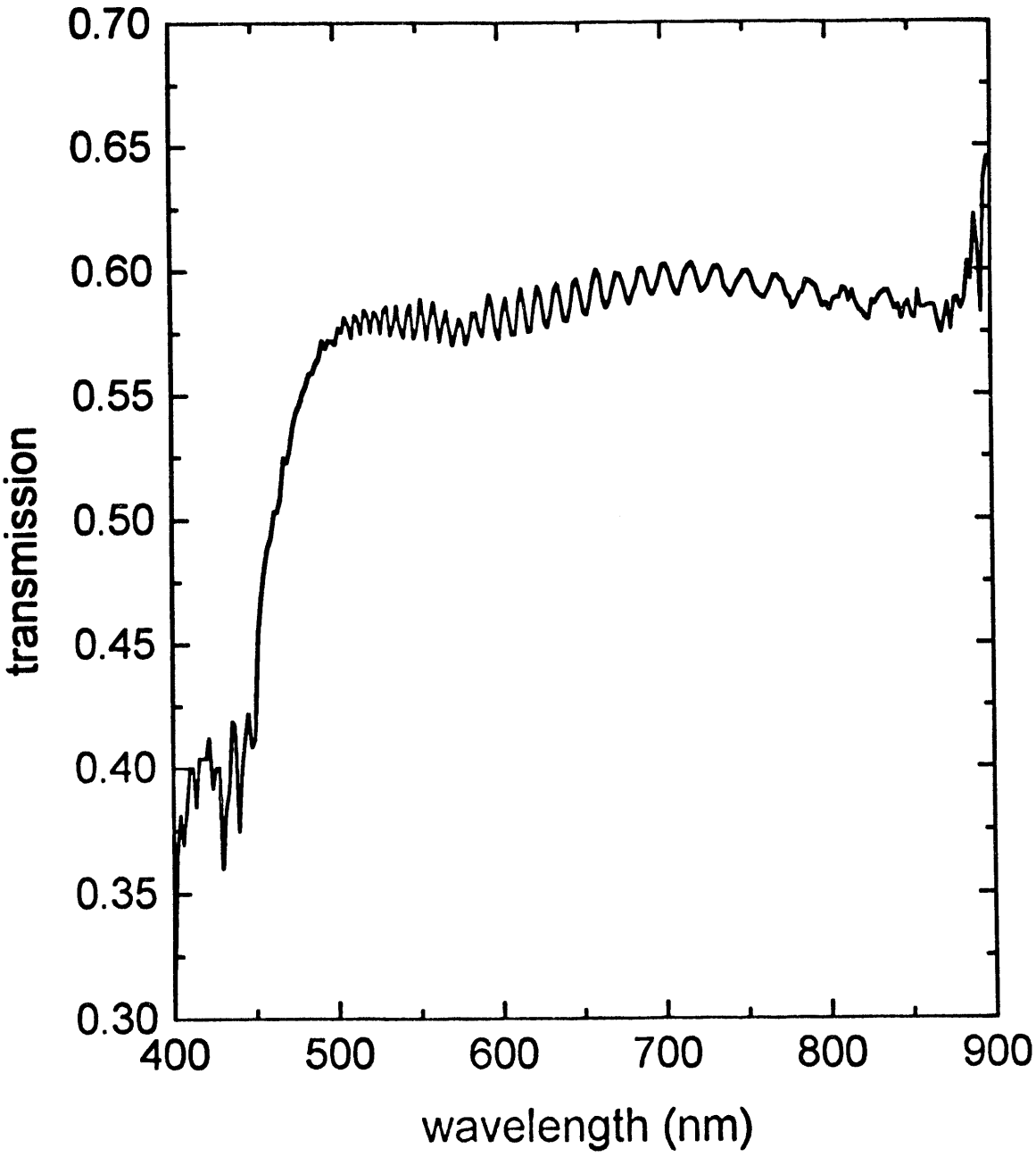
0.70
0.65
0.60
0.55
0.50
0.45
0.40
0.35
0.30
transmission
400
500
600
700
800
900
wavelength (nm)

Figure 9b

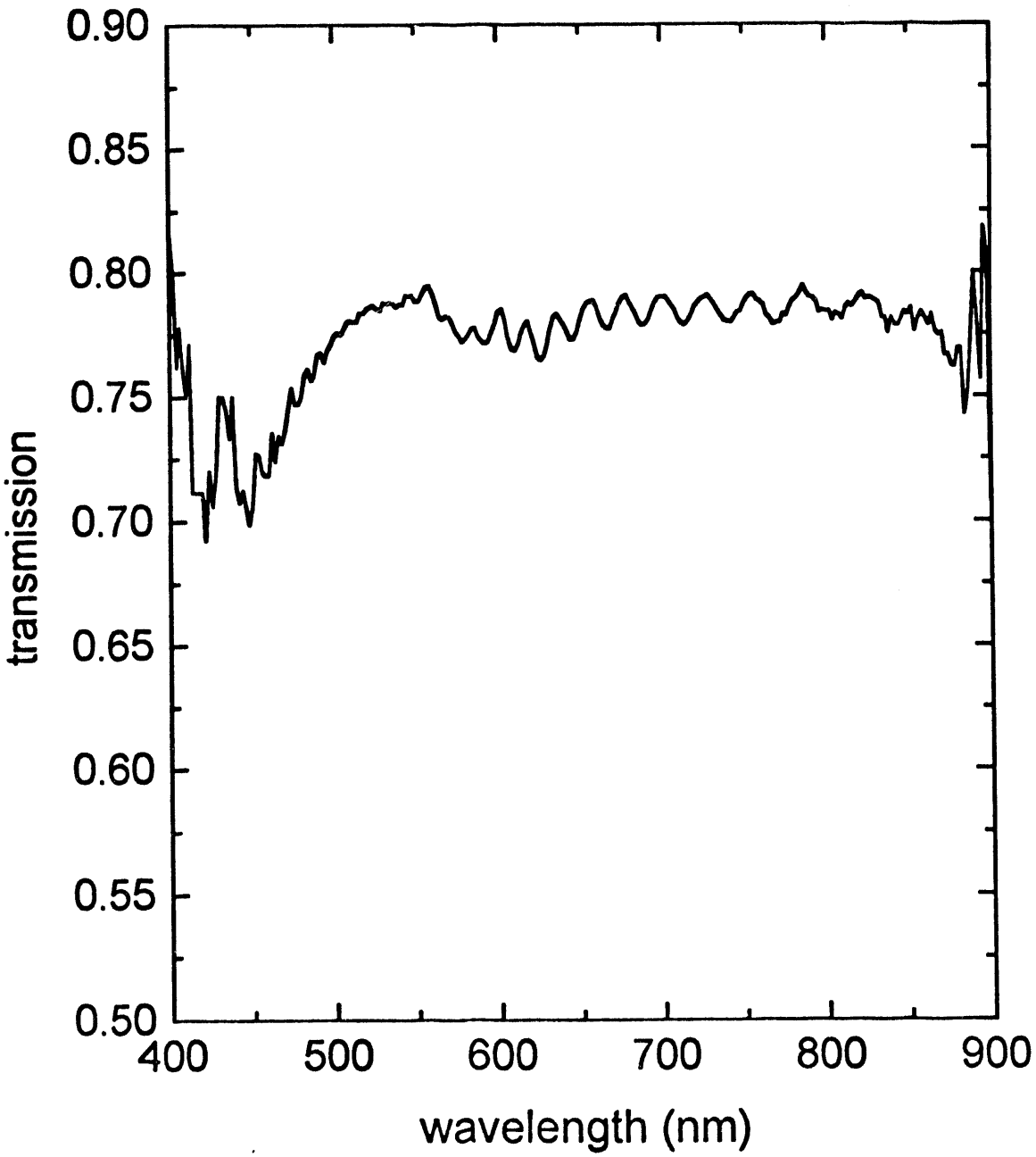
0.90
0.85
0.80
0.75
0.70
0.65
0.60
0.55
0.50
transmission
400
500
600
700
800
900
wavelength (nm)

Figure 9c

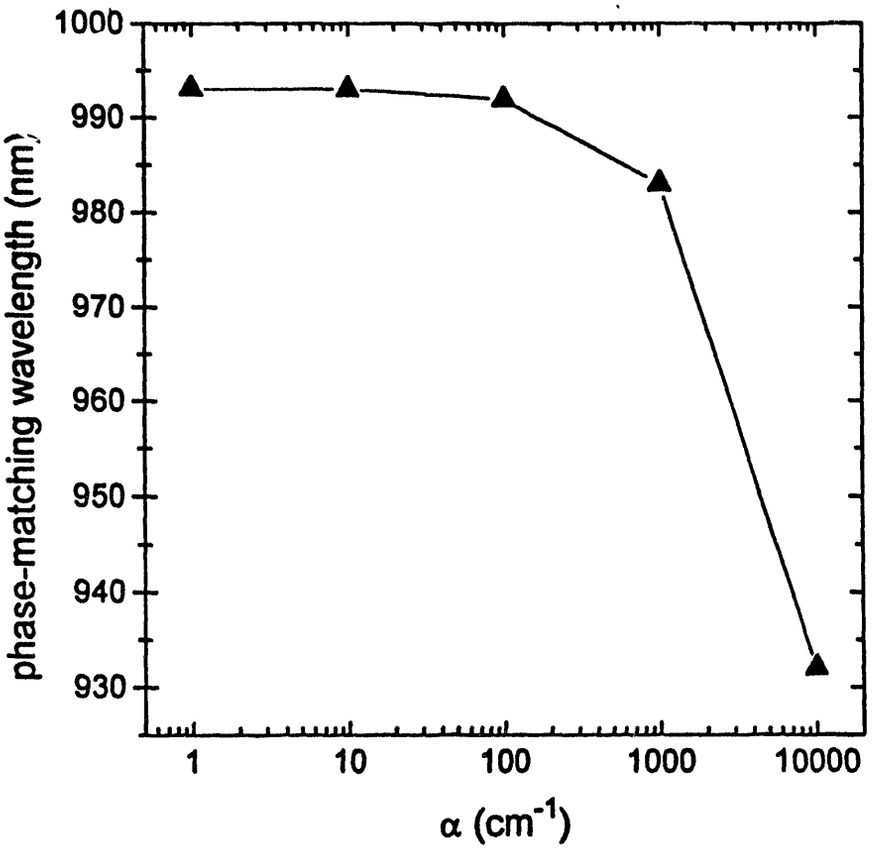
1000
990
980
970
960
950
940
930
phase-matching wavelength (nm)
1
10
100
1000
10000
α (cm-1)

Figure 10

DATE
FILMED
4/28/94
END